

PRACTICAL TECHNIQUES FOR ELASTIC SECONDARY STIFFNESS DESIGN TO PROVIDE SEISMIC STABILITY AND ENHANCE SEISMIC RESILIENCE

Larry A. Fahnestock¹, Shitao Shi¹, Rafael Sabelli², Matthew S. Speicher³

The Grainger College of Engineering, University of Illinois Urbana-Champaign, Urbana, IL USA¹

Walter P. Moore, San Francisco, CA, USA²

National Institute of Standards and Technology, Gaithersburg, MD, USA³

Abstract

Although ductility is a foundational attribute of seismic design, it is not sufficient to provide seismic stability. Instead, persistent positive tangent stiffness that obviates the destabilizing effects of gravity is the essential attribute that prevents earthquake-induced collapse of a structure even at large inelastic drifts. Many ductile seismic force-resisting systems (SFRS) develop distributed yielding of fuse elements that leads to gradual softening, maintaining positive stiffness over a significant drift range. This region of positive secondary (post-yield) stiffness provides favorable performance, although this benefit is not recognized in current standards and is thus not typically considered in design. Secondary stiffness varies between different SFRS and even within different realizations of a particular SFRS. Thus, instead of allowing the post-yield stiffness of a system to be an uncontrolled property, a more rational and reliable approach is to directly design an elastic secondary stiffness system as a companion to the primary SFRS. The secondary system is designed to have sufficient stiffness to offset the negative geometric stiffness effects while having sufficient flexibility (considering its strength) to remain elastic to large drifts. In addition to providing reliable seismic stability, the persistent elastic restoring force of the secondary stiffness system has the benefit of bringing the structure back toward its initial plumb position during dynamic earthquake response, which reduces transient and residual drifts. This paper describes a framework for designing elastic secondary stiffness systems to improve seismic performance and seismic resilience. Archetype building designs are presented and their performance is assessed with nonlinear analysis.

Introduction

The stability of a building against earthquake-induced sidesway collapse depends on the seismic force-resisting system (SFRS) equilibrating not only the effect of horizontal seismic accelerations, but also the destabilizing effect of the vertical gravity loads acting at horizontal drifts caused by those accelerations (the “P-Delta effect”). The P-Delta effect is equivalent to an additional overturning moment at each story caused by the gravity load (P) times a moment arm equal to the story drift (Δ). Figure 1 shows a schematic diagram of seismic base shear versus lateral drift for an idealized structure with story height of h . The P-Delta effect is shown as a negative stiffness line with slope $K_{P\Delta} = P/h$. The elastic structural stiffness without the P-Delta reduction is shown as a line with slope K_{e1} , and with the P-Delta reduction as a line with slope K_{e2} . Thus, K_{e2} is the effective elastic stiffness of the system in the presence of the vertical load. In the elastic range, the P-Delta effect can be considered as a reduction in effective stiffness, and both the resistance and the P-Delta effect increase linearly with drift. This permits a straightforward determination of the elastic P-Delta amplification based on the effective stiffness (K_{e2}) and equilibrium at the second-order drift. Using the stability coefficient $\theta = K_{P\Delta}/K_{e1}$, the associated amplifier $B_2 = 1/(1-\theta)$ can be used to evaluate the elastic P-Delta effect. Current code provisions in the United States (ASCE 2022) require consideration of the elastic P-Delta effect in seismic design.

However, seismic response at the Design Earthquake (DE) involves significant inelastic ductile behavior. In the inelastic range, the P-Delta effect continues to increase linearly with displacement whereas the

resistance does not. Thus, the P-Delta effect becomes proportionally much larger in the inelastic range than it is in the elastic range. Furthermore, an amplifier such as B_2 , or a more rigorous elastic analysis formulation that directly considers geometric stiffness, does not accurately capture the inelastic P-Delta effect. Figure 1 shows inelastic base shear versus drift curves, with and without the P-Delta reduction in effective strength. The figure shows that in the current design method, both required strength and estimated inelastic drift are amplified by the elastic second-order effect, represented by B_2 . The inelastic drift also utilizes the deflection amplification factor C_d , which represents the expected drift of a system designed for forces reduced by the response modification coefficient R , which accounts for ductility and overstrength. The P-Delta effect consumes a larger proportion of the inelastic lateral resistance at larger drifts, ultimately leading to negative effective stiffness as the SFRS reaches its peak strength. This condition can lead to a significant increase in drift demands (Gupta and Krawinkler 2000), making P-Delta an appreciable concern for seismic stability.

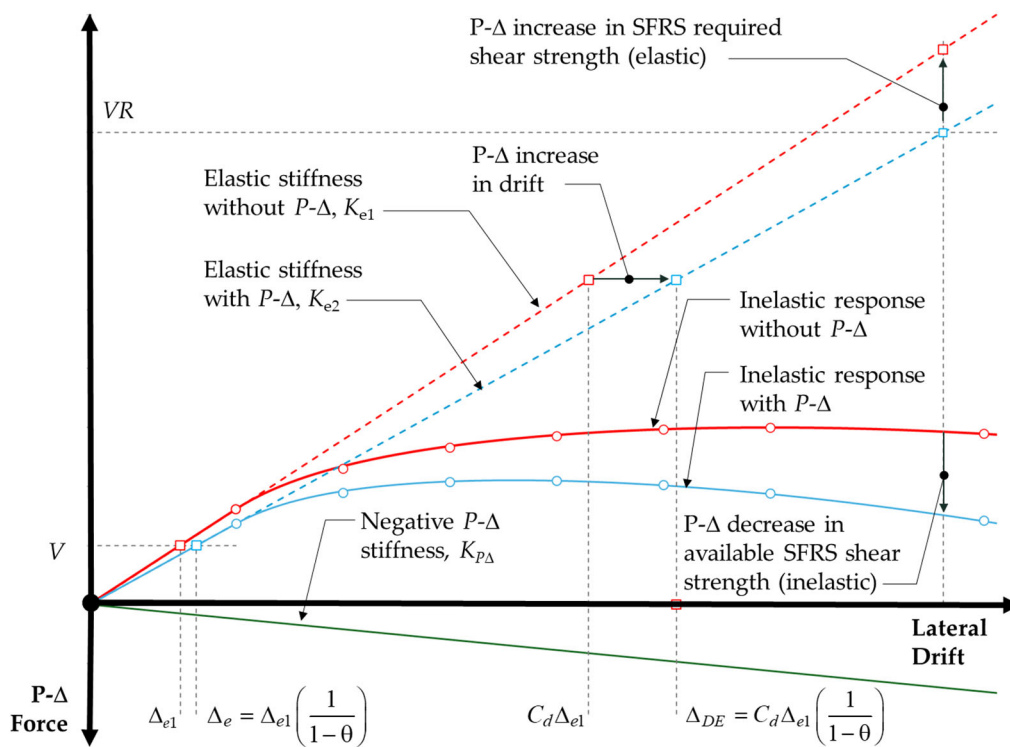


Figure 1. Seismic base shear versus lateral drift.

Since a portion of the SFRS lateral resistance is consumed in resisting the P-Delta effect, and thus the strength available to resist applied seismic loads is reduced, SFRS properties must be adjusted to compensate for the strength loss at inelastic lateral drift. Provisions in American Society of Civil Engineers (ASCE) 7-22 (ASCE 2022) lead to slightly larger design strength, based on the P-Delta effect at the elastic drift Δ_{e1} shown in Figure 1. However, this approach is not consistent with the expected inelastic drift at the Design Earthquake, Δ_{DE} , and it does not appreciably influence member proportioning or seismic response (Mathur et al. 2012). Other elements of current provisions, such as controlled strength loss in ductile systems at large inelastic drift, indirectly seek to address the P-Delta effect in the inelastic drift range. However, to more directly address the increased influence of the P-Delta effect in the inelastic drift range, a strength-based approach would need to consider a reduced effective stiffness. Such an enhanced strength-based approach – compared to current provisions in ASCE 7-22 – would improve seismic performance, but would not directly address the most fundamental parameter that

influences seismic stability, namely, persistent secondary (post-yield) tangent stiffness (Fahnestock 2022). This paper does not examine an enhanced strength-based approach for considering the P-Delta effect, but rather presents an approach for designing elastic secondary stiffness to improve seismic performance and seismic resilience.

Secondary Stiffness

Background. The importance of secondary stiffness has been known for decades. For example, MacRae (1994) identified the ratio of post-yield stiffness to elastic stiffness as the major parameter that controls dynamic stability, and Gupta and Krawinkler (2000) demonstrated the deleterious effects of global negative stiffness after significant inelastic response. Although secondary tangent stiffness has not been implemented in design provisions as a parameter that is explicitly proportioned, ductile SFRS typically develop distributed yielding that leads to gradual softening and a significant region of positive post-yield stiffness. This post-yield stiffness plays an essential role in favorable seismic performance, yet it varies between different SFRS and even within different realizations of a particular SFRS. In fact, code-compliant ductile SFRS can be configured in a way that minimizes post-yield stiffness and leads to performance that is lower than desired (Zaruma and Fahnestock 2018). Instead of allowing the post-yield stiffness of a system to be an uncontrolled parameter that varies based on other design decisions, a more direct and reliable approach is to design an elastic secondary stiffness system as a companion to the primary SFRS. The secondary stiffness system is designed to be flexible so that it can remain elastic at large drifts, but it is also proportioned to be stiff enough to combat the negative geometric stiffness effects. A recent investigation of a designed elastic secondary stiffness frame (SSF) system using diagonal braces in the context of a steel-framed building demonstrated robust results (Hariri et al. 2024). The present study is exploring an elastic SSF system using flexural response in a steel-framed building.

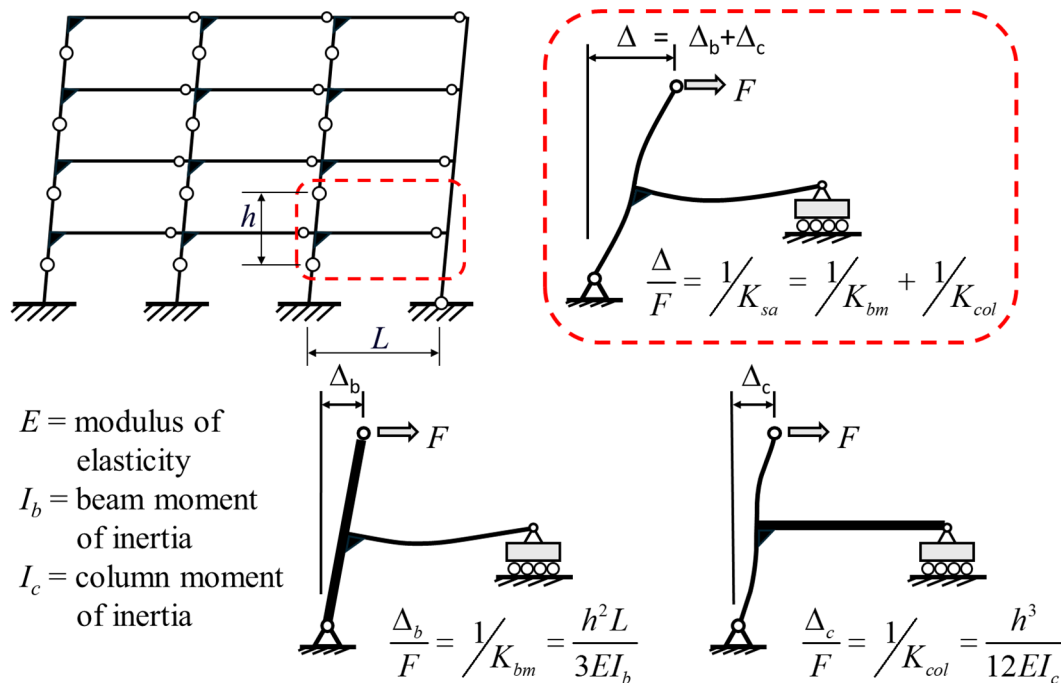


Figure 2. Schematic gravity frame and subassembly for designing secondary stiffness properties.

Implementation. Since steel-framed buildings typically have a relatively small number of SFRS bays and significantly more gravity-only bays, the gravity framing can be leveraged for elastic SSF design. Figure 2 illustrates a schematic multi-bay multi-story gravity frame where the beam-column connections are pinned (gravity shear connections), represented by a small open circle. To mobilize this gravity framing as an elastic SSF, the left end of every beam is changed from pinned to fixed (moment connections), as represented by a filled triangle. Assuming inflection points at mid-height of every column (represented by a large open circle) and the right-side column providing negligible stiffness, a subassembly is used for designing the SSF properties. The approximate lateral stiffness of the subassembly, K_{sa} , comprises beam stiffness, K_{bm} , and column stiffness, K_{col} , components as defined in Figure 2, with $K_{sa} = K_{bm}K_{col}/(K_{bm}+K_{col})$. The total number of subassemblies in a story, n , must have cumulative stiffness nK_{sa} that exceeds the destabilizing effect of gravity in the story, P_{story}/h . This requirement establishes the minimum stiffness for the SSF. Since the SSF must remain elastic up to a large drift, a maximum stiffness requirement is established for the subassembly using the estimated drift at the Maximum Considered Earthquake, Δ_{MCE} . Thus, K_{sa} must not exceed $M_{pb}/h\Delta_{MCE}$ and $2M'_{pc}/h\Delta_{MCE}$ where M_{pb} is the beam plastic moment capacity and M'_{pc} is the column plastic moment capacity adjusted for axial-flexural interaction. The minimum frame stiffness depends on the number of frames used (n), while the maximum stiffness depends on the members selected. Using more frames to achieve the same cumulative system stiffness (nK_{sa}) permits selection of lighter members and may facilitate meeting the maximum-stiffness requirement.

Theme Building

As a case study for application of the SSF concept in steel moment frames, a 12-story office building (Figure 3), was adapted from a previous 16-story design (Harris and Speicher 2015). This structure employs two three-bay Special Moment Frames (SMFs) in the east-west direction and two two-bay Special Concentrically Braced Frames (SCBFs) in the north-south direction. This study considers only the east-west direction. All interior bays are gravity framed, and these bays are strategically used to provide the SSF, which is named the secondary-stiffness moment frame (SSMF). Since this SSMF is designed to remain elastic, it does not require special detailing or capacity-based proportioning like the primary SMF. As shown in Figure 3, two three-bay SSMFs are used for this case study. The building is located in Los Angeles, California (33.821° N, 117.818° W) and designed using the ASCE 7-22 equivalent lateral force (ELF) procedure along with the appropriate steel standards as follows: American Institute of Steel Construction (AISC) 360-22 (AISC 2022b), AISC 341-16 (AISC 2016), and AISC 358-22 (AISC 2022a).

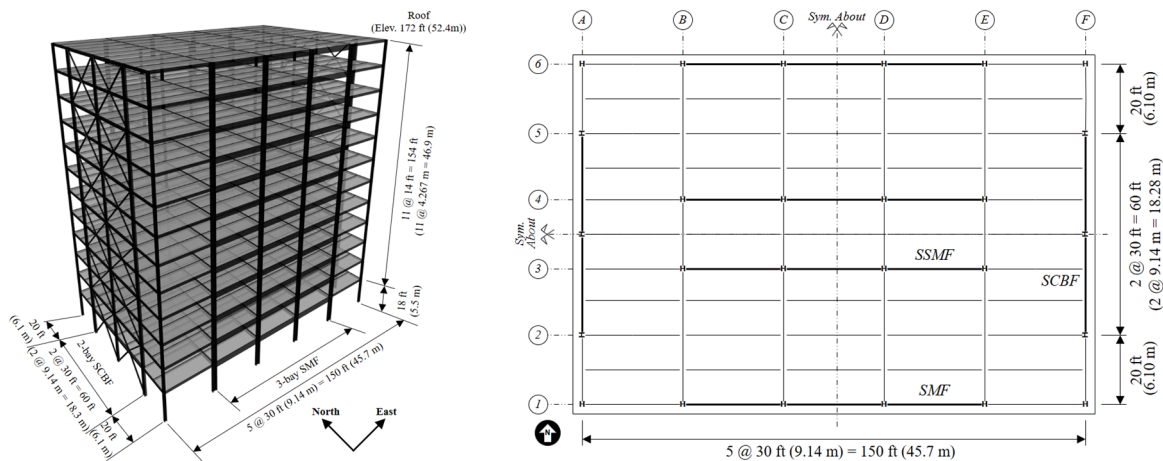


Figure 3. 12-story theme building: isometric view and floor plan.

Numerical Modeling Methodology

Analyses were executed using the OpenSees platform (McKenna et al. 2010), including elastic analyses for structural proportioning and nonlinear inelastic static and dynamic analyses for performance assessment. All models are two-dimensional based on structural symmetry and a rigid diaphragm assumption. Nonlinear models follow established procedures (NIST 2017, Speicher et al. 2020), where all beams and columns in the SMFs and SSMFs are modeled as elastic elements with nonlinear rotational springs at the ends, and nonlinear panel zone behavior is represented at all beam-column joints. Modal damping of 2 % is used, supplemented by 0.1 % stiffness-proportional damping to mitigate higher modes of vibration. A leaning column captures the destabilizing effects of gravity, and it has flexural stiffness and strength properties associated with the summation of all columns tributary to the SFRS.

Seismic Design Case Study

The design matrix includes three cases, all of which satisfy a 2 % story drift limit per ASCE 7-22. The first case, referred to as Baseline SMF (two three-bay SMFs, on Column Lines 1 and 6), is proportioned using first-order elastic analysis and thus does not account for the P-Delta effect. The second case, called Current Practice SMF (two three-bay SMFs, on Column Lines 1 and 6), is proportioned using second-order elastic analysis, which accounts for the P-Delta effect at a small elastic drift as required in current provisions, although this is not a robust approach as discussed above. In both of these cases, gravity-only framing is on Column Lines 3 and 4. The third case, referred to as Baseline SMF plus SSMF, employs an enhanced SSMF gravity frame that is proportioned as described above and replaces the gravity-only framing on Columns Lines 3 and 4 as illustrated in Figure 3. For the SMF, A992 wide flange sections with $F_y = 50$ (340) ksi (MPa) are used. In the SSMF, A913 Grade 65 wide flange sections with $F_y = 65$ (448) ksi (MPa) are used as a strategy to help meet the minimum and maximum stiffness requirements.

Table 1. Section Sizes for Frame Designs.

Story	Baseline SMF			Current Practice SMF			SSMF	
	Beam	Int. Column	Ext. Column	Beam	Int. Column	Ext. Column	Beam	Column
12	W24X55	W14X132	W14X132	W24X55	W14X159	W14X132	W16X26	W14X26
11	W24X84	W14X132	W14X132	W27X94	W14X159	W14X132	W18X35	W14X26
10	W27X94	W14X233	W14X159	W27X94	W14X283	W14X193	W21X44	W14X53
9	W30X124	W14X233	W14X159	W33X141	W14X283	W14X193	W21X50	W14X53
8	W30X124	W14X283	W14X211	W33X141	W14X311	W14X211	W24X55	W14X74
7	W33X141	W14X283	W14X211	W33X152	W14X311	W14X211	W24X62	W14X74
6	W33X141	W14X311	W14X233	W33X152	W14X342	W14X257	W24X68	W14X99
5	W33X141	W14X311	W14X233	W33X169	W14X342	W14X257	W24X76	W14X99
4	W33X141	W14X311	W14X233	W33X169	W14X370	W14X283	W24X84	W14X132
3	W33X141	W14X311	W14X233	W33X169	W14X370	W14X283	W24X94	W14X132
2	W33X141	W14X342	W14X283	W33X169	W14X398	W14X342	W24X103	W14X176
1	W33X141	W14X342	W14X283	W33X169	W14X398	W14X342	W27X129	W14X176

Steel weight comparisons for a single frame (a three-bay moment frame, one half of the SFRS in one direction) provide a reasonable estimate of relative cost for the three design cases considered here. The Baseline SMF weighs 297 (1320) kips (kN) and the Current Practice SMF weighs 340 (1510) kips (kN).

Thus, current design provisions lead to approximately a 15 % SMF steel weight increase due to the P-Delta effect. The SSMF is an enhanced version of a three-bay line of gravity framing (e.g. Column Line 3 from Column Lines B to E), as shown in Figure 3. As a gravity-only frame (A992 steel), the steel weight for this line of framing is 116 (516) kips (kN), and when it is enhanced to serve as the SSMF (A913 Grade 65 steel), the steel weight is 140 (623) kips (kN). Assuming a 10 % premium for the higher strength steel in the SSMF, the equivalent A992 SSMF frame weight for cost comparison is 154 (685) kips (kN). Thus, to obtain a comparable steel weight that is associated with SFRS cost, the increase in weight from gravity-only to SSMF, 38 (169) kips (kN), is added to the Baseline SMF to obtain 335 (1490) kips (kN). Thus, the Baseline SMF plus SSMF is slightly more economical than the Current Practice SMF, and as will be shown below, it has significantly better performance.

Nonlinear Assessment

Static Response. To evaluate inelastic behavior of the three design cases, displacement-controlled nonlinear static analyses were conducted (Figure 4). The Baseline case was assessed with no gravity load on the leaning column. Thus, it serves as a reference case where the P-Delta effect is not included in proportioning or assessment, and it can be viewed as a target for a design method to achieve perfect correction for the P-Delta effect. Figure 4 indicates Current Practice case does not adequately compensate for the P-Delta effect, as it does not reach the same strength levels and drift ratios as the Baseline case. The Baseline case reaches maximum base shear around 2.7 % roof drift ratio, whereas Current Practice reaches maximum base shear around 1.4 % roof drift ratio. The maximum base shear in Current Practice compared to Baseline is around 90 %. In contrast, the SSMF case, which is the Baseline SMF design plus the SSMF, provides significant secondary stiffness and counteracts the P-Delta effect, reaching maximum base shear around 3.2 % roof drift ratio. The peak base shear for SSMF is around 130 % of Baseline. Figure 4 reveals that Baseline exhibits an extended region of positive secondary stiffness extending across a range of approximately 2 % roof drift ratio. Current Practice is dominated by the P-Delta effect and exhibits a limited region of positive secondary stiffness extending across a range of approximately 0.5 % roof drift ratio. As anticipated, the case where secondary stiffness was explicitly designed exhibits the most prominent region of positive secondary stiffness extending across a range of more than 2 % roof drift ratio.

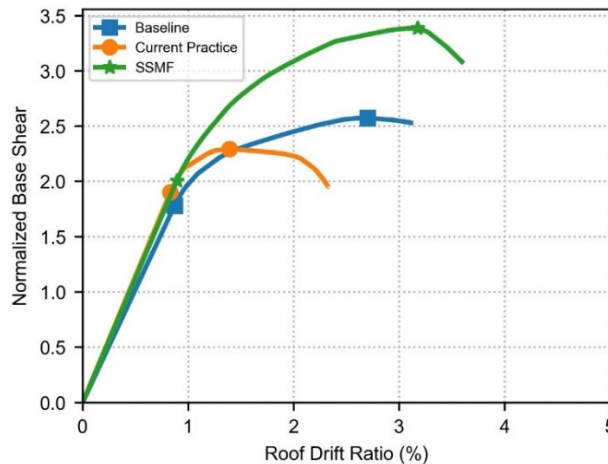


Figure 4. Normalized monotonic static pushover curves.

Dynamic Response. For nonlinear response history analysis, the Federal Emergency Management Agency (FEMA) P695 (FEMA 2009) far-field record set, which comprises 22 seismic records (44 individual components) was normalized according to FEMA P695 guidelines and scaled to the risk-targeted Maximum Considered Earthquake (MCE_R) response spectrum at the fundamental period of the SFRS. As a case study, the system responses to the acceleration record Imperial Valley, El Centro Array #11 (IMPVALL/H-E11140) are illustrated in Figure 5. Although all three cases have similar maximum roof drift, Current Practice, which is characterized by the smallest secondary stiffness region, develops significant residual roof drift. The reason for this is further illustrated in Figure 6, which focuses on first story drift. SSMF has a similar response to Baseline, but Current Practice develops a very large first story drift that exceeds the 7.5 % threshold and is considered to indicate collapse in this study. Near the end of the record the response is trending toward complete sideways collapse.

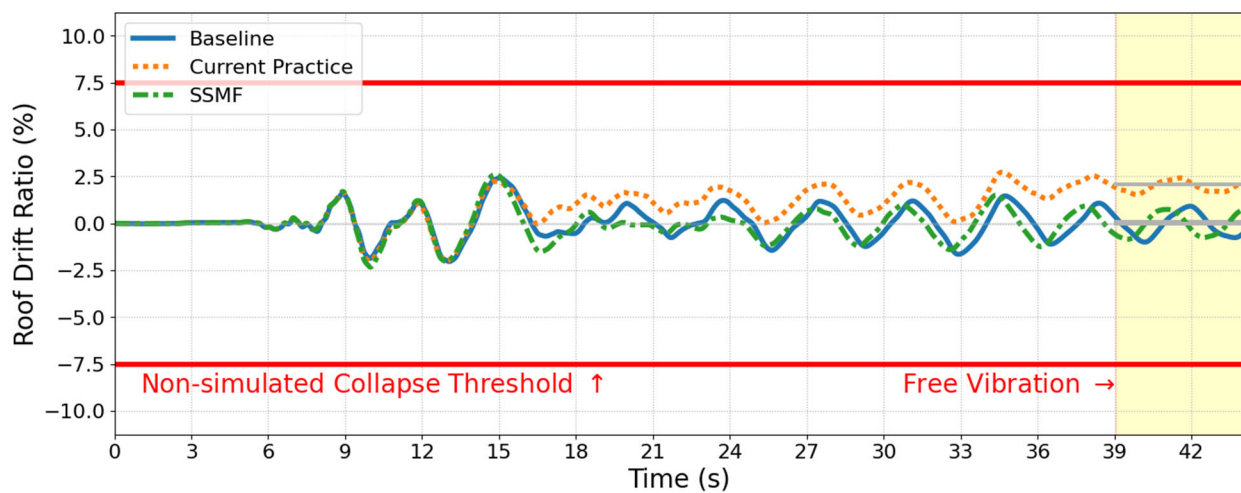


Figure 5. Roof drift ratio response history for SMFs subjected to Imperial Valley, El Centro Array #11 (IMPVALL/H-E11140) scaled to MCE_R .

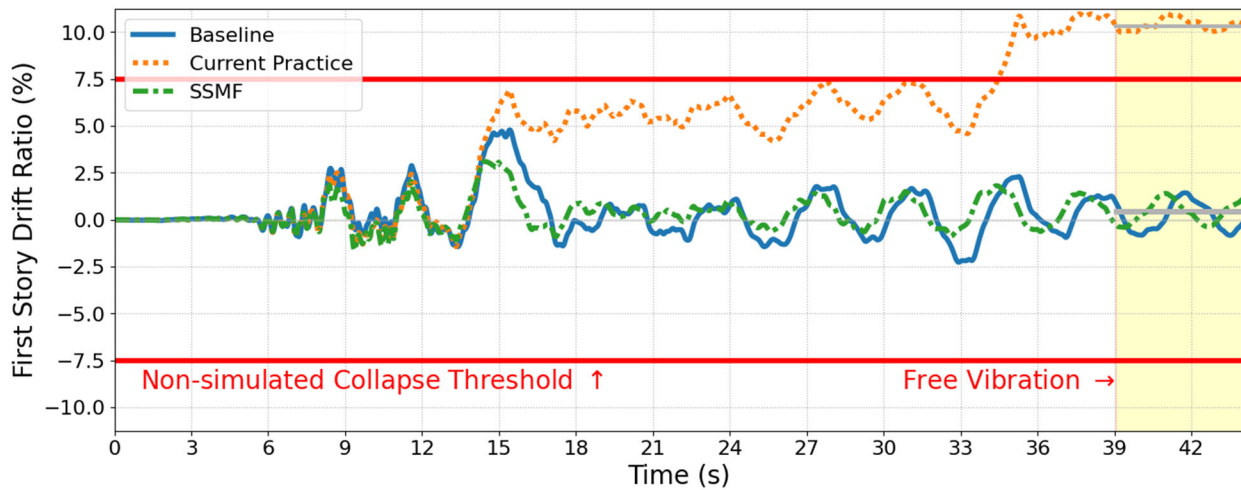


Figure 6. First story drift ratio response history for SMFs subjected to Imperial Valley, El Centro Array #11 (IMPVALL/H-E11140) scaled to MCE_R .

Summary

This paper presents an approach for designing elastic secondary stiffness moment frames that counteract the P-Delta effect and provide seismic stability. Case study designs illustrate the performance of current practice special moment frames (SMF) and SMFs enhanced with elastic secondary stiffness moment frames (SSMF). Evaluated statically, the Current Practice SMF has minimal intrinsic secondary stiffness whereas the combined SMF (proportioned ignoring the P-Delta effect) and SSMF has an extensive region of secondary stiffness. The Current Practice SMF does not effectively counteract the P-Delta effect, whereas the combined SMF and SSMF does. Dynamic response indicates that the combined SMF and SSMF can reduce maximum and residual drift compared to the Current Practice SMF, and that it performs better than the hypothetical case without the P-Delta effect. This initial study illustrates the promise of using elastic secondary-stiffness moment frames as an economical and simple approach for providing seismic stability and enhancing seismic resilience. Future research is needed to comprehensively quantify the influence of secondary-stiffness moment frames on seismic performance of a broader range of primary SFRS and to develop an implementation strategy for design provisions.

References

- AISC, 2016, "Seismic Provisions for Structural Steel Buildings," ANSI/AISC 341-16, American Institute of Steel Construction, Chicago, IL, USA.
- AISC, 2022a, "Prequalified Connections for Special and Intermediate Steel Moment Frames for Seismic Applications," ANSI/AISC 358-22, American Institute of Steel Construction, Chicago, IL, USA.
- AISC, 2022b, "Specification for Structural Steel Buildings," ANSI/AISC 360-22, American Institute of Steel Construction, Chicago, IL, USA.
- ASCE, 2022, "Minimum Design Loads for Buildings and Other Structures," ASCE/SEI 7-22, American Society of Civil Engineers, Reston, VA.
- FEMA, 2009, "Quantification of building seismic performance factors," FEMA P695, Federal Emergency Management Agency, Washington, DC, USA.
- Fahnestock, L.A., 2022, "Seismic Stability from Low Ductility to Enhanced Resilience," SDSS 2022 – The International Colloquium on Stability and Ductility of Steel Structures, Aveiro, Portugal, September 2022.
- Gupta, A, and Krawinkler, H., 2000, "Dynamic P-Delta Effects for Flexible Inelastic Steel Structures," *Journal of Structural Engineering*, ASCE, 126 (1): 145–154.
- Hariri, B., Christopoulos, C., and Tremblay, R. 2024, "Design Guidelines for Mitigating P-Delta Effects on the Seismic Response of Multi-Storey Steel Building Structures in Moderate and High Seismic Regions," 2024 SSRC Annual Stability Conference, San Antonio, TX, USA, March 2024.
- Harris III, J.L., Speicher, M.S., 2015, "Assessment of First Generation Performance-Based Seismic Design Methods for New Steel Buildings, Volume 1: Special Moment Frames," NIST Technical Note 1863-1, National Institute of Standards and Technology, Gaithersburg, MD, USA.
- Ibarra, L.F., Medina, R.A., Krawinkler, H., 2005, "Hysteretic models that incorporate strength and stiffness deterioration," *Earthquake Engineering and Structural Dynamics*, 34(12), pp. 1489-1511.

- MacRae, G.A., 1994, "P- Δ Effects on Single-Degree-of-Freedom Structures in Earthquake," *Earthquake Spectra*, EERI, 10 (3): 539-568.
- Mathur, K., Fahnestock, L.A., Okazaki, T. and Parkolap, M.J., 2012, "Impact of Residual Stresses and Initial Imperfections on the Seismic Response of Steel Moment Frames," *Journal of Structural Engineering*, ASCE, 138 (7): 942-951.
- McKenna, F., Scott, M.H., Fenves, G.L., 2010, "Nonlinear finite-element analysis software architecture using object composition," *Journal of Computing in Civil Engineering*, 24(1), pp. 95-107.
- NIST, 2017, "Guidelines for nonlinear structural analysis and design of buildings: Part IIa - steel moment frames," NIST GCR 17-917-46v2, National Institute of Standards and Technology, Gaithersburg, MD, USA.
- Speicher, M.S., Dukes, J.D., Wong, K.W., 2020, "Collapse Risk of Steel Special Moment Frames per FEMA P695," NIST Technical Note 2084, National Institute of Standards and Technology, Gaithersburg, MD, USA.
- Zaruma, S. and Fahnestock, L.A. 2018, "Assessment of design parameters influencing collapse performance of buckling-restrained braced frames," *Soil Dynamics and Earthquake Engineering*, 113 (2018) 35-46.